

## Department of Mechanical Engineering and Mechanics

### Drexel University College of Engineering

The following item is made available as a courtesy to scholars by the author(s) and Drexel University Library and may contain materials and content, including computer code and tags, artwork, text, graphics, images, and illustrations (Material) which may be protected by copyright law. Unless otherwise noted, the Material is made available for non profit and educational purposes, such as research, teaching and private study. For these limited purposes, you may reproduce (print, download or make copies) the Material without prior permission. All copies must include any copyright notice originally included with the Material. **You must seek permission from the authors or copyright owners for all uses that are not allowed by fair use and other provisions of the U.S. Copyright Law.** The responsibility for making an independent legal assessment and securing any necessary permission rests with persons desiring to reproduce or use the Material.

Please direct questions to [archives@drexel.edu](mailto:archives@drexel.edu)

Drexel University Libraries  
[www.library.drexel.edu](http://www.library.drexel.edu)



<http://www.drexel.edu/>

# 3D Microtomographic Characterization of Precision Extruded Poly- $\epsilon$ -caprolactone Scaffolds

A. L. Darling, W. Sun

Laboratory for Computer-Aided Tissue Engineering, Department of Mechanical Engineering and Mechanics, Drexel University, 3141 Chestnut Street, Philadelphia, Pennsylvania 19104

Received 21 October 2003; revised 19 December 2003; accepted 23 December 2003

Published online 6 April 2004 in Wiley InterScience (www.interscience.wiley.com). DOI: 10.1002/jbm.b.30050

**Abstract:** One of the dominant approaches to tissue engineering is the seeding of biodegradable, biocompatible polymer scaffolds with progenitor cells prior to 3D culture or implantation. The microarchitecture of these scaffolds has direct effects upon the ability of cells to attach, migrate, and differentiate. Microtomographic (micro-CT) scanners enable high-speed 3D characterization of the salient features of these polymer scaffolds. A micro-CT scan followed by 3D reconstruction of serial image sections can determine porosity, pore size, pore interconnectivity, strut size, and overall 3D microarchitecture. In this study, four polymer samples with different microarchitectures were manufactured through precision extrusion deposition free-form fabrication and subsequently characterized through micro-CT analysis. A desktop micro-CT scanner was used to examine each sample at approximately 19.1-micron resolution. 2D analyses and 3D reconstructions of core regions of each sample were performed. These results illustrate that qualitative and quantitative analysis of polymer scaffolds is possible using micro-CT and 3D reconstruction techniques. © 2004 Wiley Periodicals, Inc. *J Biomed Mater Res Part B: Appl Biomater* 70B: 311–317, 2004

**Keywords:** micro-CT; tissue engineering; porosity; polycaprolactone; microarchitecture

## INTRODUCTION

Constructing polymer scaffolds followed by seeding of progenitor cells has proven to be one of the most effective techniques in tissue engineering. The subsequent 3D culture and implantation of these biocompatible, biodegradable scaffolds has found widespread experimental and limited clinical use. The design of such scaffolds permits culture of these tissues in structures with porosity, surface area, and surface characteristics optimized for each tissue type cultured. Fine control of these microarchitectural characteristics also influences the mechanical properties of the scaffold, important for tissues for which mechanotransduction is a proliferative control.

Tissue engineering scaffolds benefit from a porous structure, whether being used to seed cells *in vitro* prior to implantation or as conductive structures *in vivo*. Typical desirable porosities for tissue engineering scaffolds are around 90%, with pore sizes in the range of 100–200 microns.<sup>1</sup> The cells utilize the additional surface area for attachment and

thrive in an environment where extracellular fluids can circulate freely. In addition, interconnectivity of these pores allows greater circulation of extracellular material, connection between neighboring cells, and increased ease of cell migration.<sup>2</sup> Techniques for creating or accentuating the porous structure of polymer scaffolds include casting the scaffolds in assemblies of paraffin spheres to create a uniform density of spherical pores and expanding pore size and interconnectivity through salt fusion.<sup>2,3</sup> One of the drawbacks in traditional approaches to scaffold manufacture has been the inability to ensure that channels and pores interconnect, resulting in regions in the scaffold where tissue survival, much less growth, is impossible.<sup>4</sup>

The ability to evaluate porous scaffold structures for porosity, pore size, and pore interconnectivity in a timely manner would be quite valuable for tissue engineering. In this article, we demonstrate the analysis of scaffolds for structural tissue engineering requirements using microtomography (micro-CT). Micro-CT can be utilized to nondestructively quantify a sample according to microarchitectural criteria. Micro-CT scans image the target through exposure to small quantities of ionizing radiation and measurements of absorption. The resulting gray-scale images are a series of sequential slices depicting a density map of the scanned sample. 3D reconstruction of these serial slices can reproduce a model of the interior of the original sample. In this study, we analyzed four polymer scaffolds, quantifying their tissue engineering

Correspondence to: W. Sun, Laboratory for Computer-Aided Tissue Engineering, Department of Mechanical Engineering and Mechanics, Drexel University, 3141 Chestnut Street, Philadelphia, Pennsylvania 19104 (e-mail: sunwei@drexel.edu)

Contract grant sponsor: the National Science Foundation; contract grant number: 0219176

© 2004 Wiley Periodicals, Inc.

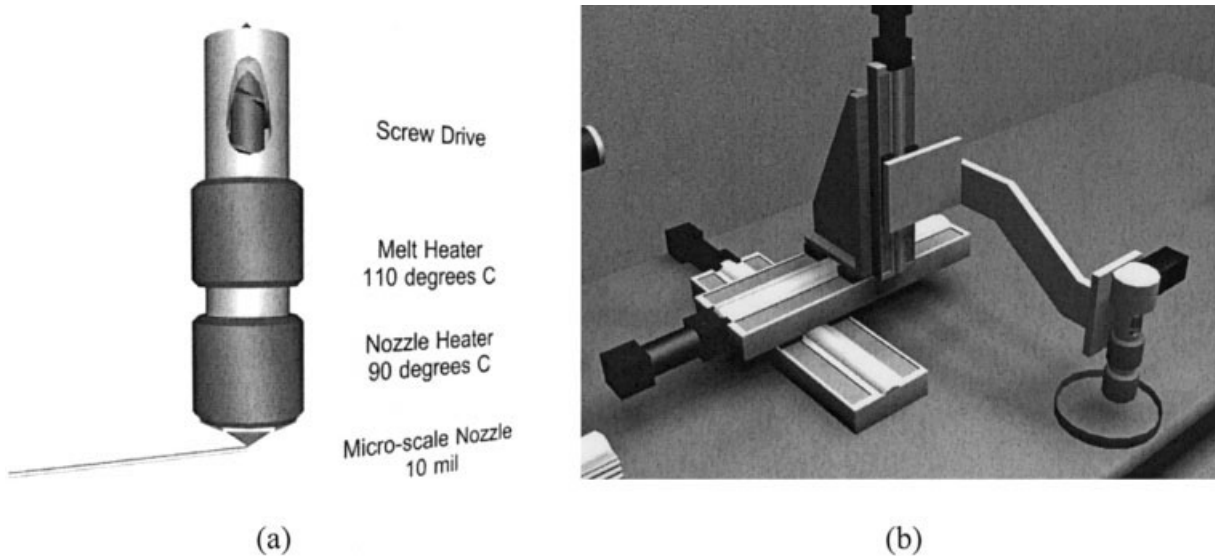


**Figure 1.** The Precision Extrusion Deposition system: (a) extrusion head, and (b) 3D positioning assembly.

specific criteria and reconstructing a model of their interiors from tomographic data.

## MATERIALS AND METHODS

### Preparation of Polymer Scaffolds

The samples were prepared through precision extrusion deposition manufacturing, a rapid prototyping technique whereby polymer is deposited in strands using a three-dimensional positioning system and a heated extrusion head.<sup>5</sup> Poly- $\epsilon$ -caprolactone (PCL) was selected for biocompatibility and ease of manufacture. PCL is a biocompatible polymer for which extensive biocompatibility and efficacy studies have been performed *in vitro* and *in vivo*.<sup>6–8</sup> It is a semicrystalline aliphatic polymer that has a slower degradation rate than most biopolymers in its homopolymeric form. PCL has an unusually low melting temperature of about 58–60°C with a high thermal stability. This low melting temperature enables a pair of heating elements in the extrusion head to melt the polymer

quickly and maintain it in the liquid state in the nozzle head. Pressure is generated in the nozzle and more material is fed into the heating chamber by a rotating screw drive.<sup>8</sup> The extrusion head and positioning assembly are illustrated in Figure 1.

The toolpath for the extrusion head was generated using commercially available software. The initial model used was a cylinder in stereolithography (STL) format, a standard surface represented format by which the surface is defined by triangles. The slicing software divided the model into layers of 254 microns in height, then subsequently established a toolpath for each slice. The toolpath consisted of a single deposition path doubling back upon itself many times to form a series of parallel lines. The toolpath for the next layer was angled 60 degrees relative to the previous layer and at a 254-micron higher elevation. A sample conversion from the STL format to the toolpath is shown in Figure 2. The primary variable in the design of the toolpath is a fill gap, the distance between the parallel lines of the toolpath. The toolpath is then exported as a Numerical Control (NC) code to the 3D posi-

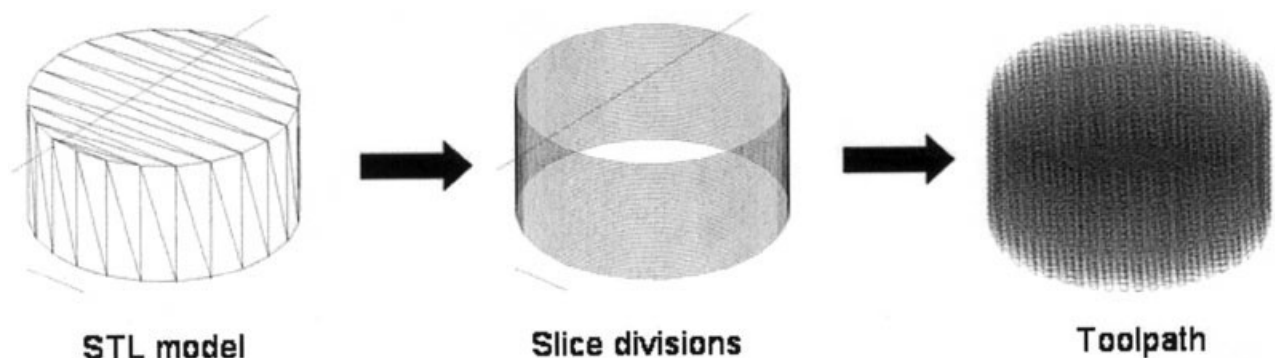


**Figure 2.** Division of STL model into a layered toolpath.

**TABLE I. Parameters for PCL Sample Manufacture**

Sample No.	Fill Gap	Remarks
1	0.420 mm	Constant fill gap (39 layers)
2	0.510 mm	Constant fill gap (39 layers)
3L	0.510 mm/	Varying fill gap (20 layers each)
3U	0.420 mm	

Slice thickness = 0.254 mm, liquefier temperature = 110°C, nozzle heater temperature = 90°C, 10 mil nozzle tip traveling at 20 mm/s.

tioning system using in-house software. Variables in the NC code other than the toolpath include lateral velocity of the extrusion head, layer height, and rotation speed of the screw drive. Hardware parameters of the PED system include size of the microscale nozzle installed and the temperature settings of the two heaters in the system.

For this experiment, the strands were laid down in three distinct layering patterns, designated 1, 2, and 3, alternating strand layers of 0° and 60°. Samples 1 and 2 have uniform fill gap widths between parallel lines in the toolpath of a single layer. Sample 3 consists of two layout patterns, a low-density/high fill gap width pattern designated 3L in the lower half and a high-density/low fill gap width pattern designated 3U in the upper half. Toolpath, NC code, and hardware parameters for the construction of these scaffolds are displayed in Table I. An image and SEM micrographs of one of the produced scaffolds are displayed in Figure 3.

### Micro-CT Analysis

Three sample cylinders were prepared, approximately 19.5 mm in diameter and 10 mm in height, designated samples 1, 2, and 3, each with different microarchitectures. Sample 3 was a composite of two separate microarchitectures, the upper half designated 3U and the lower half designated 3L. This heterogeneous cylinder was scanned once but analyzed as two separate structures, illustrating the capacity of micro-CT to differentially analyze adjacent regions of the same scaffold.

The samples were scanned using a SkyScan 1072 micro-CT desk scanner. This is a fan-beam scanner with a focal spot size of several microns operating at 100 kV. The sample was placed on a clay mount and rotated through 360 degrees around the axis of the sample cylinder. An absorption image is taken at each point of rotation, and an absorption value is obtained for each voxel through convolution and back projection.<sup>10</sup> Although Muller et al. expressed a need for a constrained Gaussian filter to reduce noise and an X-ray contrast agent to enhance absorption by the radio transparent polymer in a similar experiment, neither measure was deemed necessary for these samples because of the polymer's uniformity and the dramatic contrast between the polymer and air.<sup>11</sup>

The output format for each sample was 500 serial 1024 × 1024 bitmap images. These slice images were viewed in SkyScan's Tview software. All of the 2D and 3D analysis, aside from 3D core reconstruction, was performed with

Tview. Initially, length measurements were taken around the sample to determine the degree to which the sample conformed to the cylindrical template. As each sample had a 1.3-mm ring of blurred deposition around the periphery of the cylinder, the volume analyses were performed on an elliptical region just within this periphery. Volume fraction and surface per unit volume was determined in Tview 3D analysis, and relative area was measured in 10 randomly selected slice images in Tview 2D analysis. Also, strut and pore widths were measured in 2D images from each sample, 10 random struts, and 10 random pores selected.

### 3D Reconstruction

An output format of serial bitmap images enables 3D volumetric reconstruction to be performed. 3D reconstruction operates by ascribing a height to each pixel in a bitmap image to represent a volume unit, a voxel. By stacking these bitmap images at the appropriate voxel height, a 3D model is described. Grayscale intensity thresholds may be established,

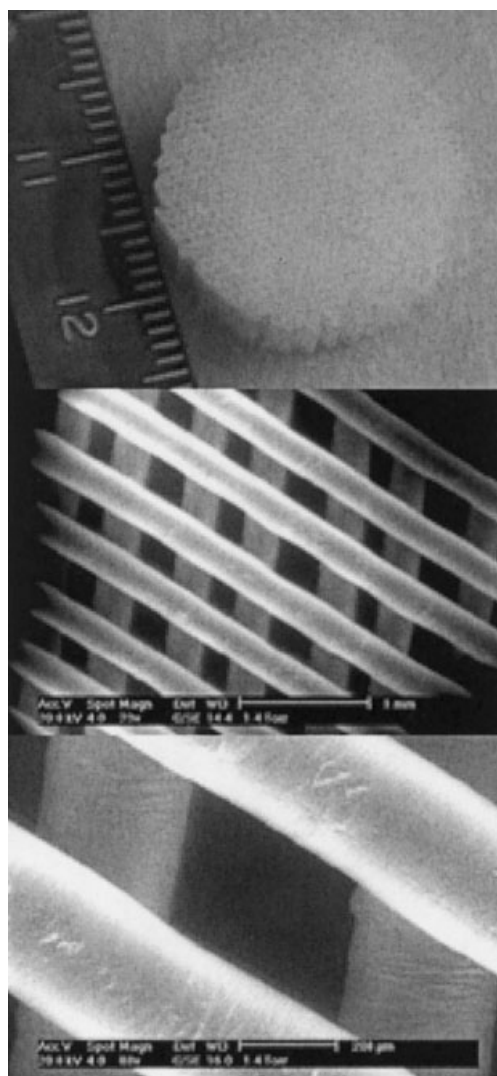


**Figure 3.** Image and SEM micrograph of sample 2.

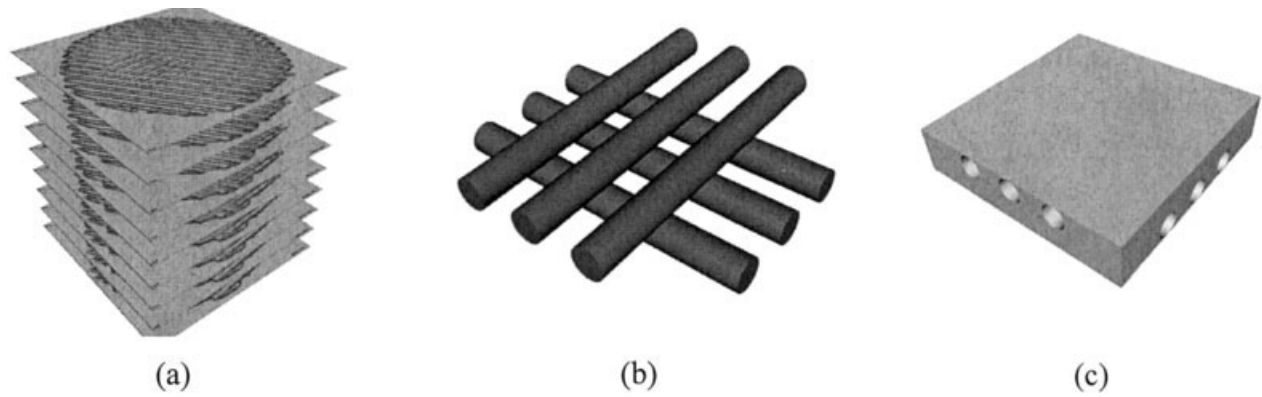


**Figure 4.** Diagram of 3D volumetric reconstruction: (a) the bitmap slices with a height ascribed to each pixel, (b) the gray scale thresholds set to establish a positive space model of sample struts, and (c) the thresholds inverted to establish a negative space model of the pore space.

selecting only voxels of a specified grayscale range to reconstruct in 3D. As such, by selecting darker thresholds, the struts of a sample may be reconstructed. Conversely, by selecting the white levels of the bitmap images, a model can be created of only the negative space, the pores of the samples in this study. A diagrammatic example of 3D reconstruction is shown in Figure 4, with (a) representing the stacked bitmap images, (b) representing the positive space of a few struts in the sample by selecting a darker gray-scale threshold range, and (c) representing the negative space, or pore space, by selecting a lighter threshold range.

3D reconstruction was performed using Materialise Mimics software with preprocessing using ImageJ shareware. Sixty-two sequential  $200 \times 200$  pixel images were cropped from the serial images of samples 1, 2, 3L, and 3U. These cores were selected from the center of each sample. Imported into Mimics, these core images were reconstructed into 3D volumetric models. The 3D reconstructed cores were then used to determine the degree of interconnectivity of the pores. Thresholds of the gray scale images were inverted to allow measurement of the volume of all pore spaces. Subsequently, a region-growing operation was performed, creating a mask consisting only of interconnected pore spaces. Volume for this region-grown mask was also determined, and the ratio of region grown volume to total volume calculated. This percentage is described as the degree of interconnectivity.<sup>12</sup>

### Cell Culture

A simple cell culture experiment was performed to determine simple biocompatibility of PCL post heating. Two sample cylinders with  $90^\circ$  strut orientation were fabricated and seeded with rat cardiomyoblasts,  $10^5$  H9C2 cells. One scaffold was filled with fibrin to assist cells in migrating across the pores, and one was left unfilled. The scaffolds were seeded, then maintained in incubation for 7 days. The scaffolds were then examined optically.

### RESULTS

Visibly, the scaffold channels appeared to extend through the entirety of the cylinder in both horizontal and vertical axes, and the strand layout in each layer seemed consistent during assembly. At the edge of the cylinder, as the strand curved back into the model to create a new strut, a region of thick and blurred deposition was visible. This region was approximately 1.3 mm at the edge of the cylinder. Also, the scaffold appeared slightly compressed in one direction. From the SEM micrograph shown in Figure 3, the strut and pore widths were seen to be around 250 microns.

A summary of data retrieved from analysis through Tview is displayed in Table II. The samples were found to be

**TABLE II. Summary of the Morphological Analysis**

Sample	3U	3L	2	1
Max./min. diameter (mm)	19.74/18.79	19.56/18.57	19.44/18.51	19.62/18.59
Surface ( $\text{mm}^2$ ) rel. area	9219	10036	18936	20854
Relative area	60.89%	44.24%	47.28%	55.8%
Total vol. ( $\text{mm}^3$ )	490	458	957	1004
Volume fraction	60.8%	45.1%	47.4%	53.1%
Porosity	39.2%	54.9%	52.6%	46.9%
Strut width ( $n = 10$ , mm)	$0.264 \pm 0.023$	$0.250 \pm 0.034$	$0.270 \pm 0.019$	$0.264 \pm 0.023$
Pore width ( $n = 10$ , mm)	$0.196 \pm 0.054$	$0.292 \pm 0.04$	$0.254 \pm 0.034$	$0.210 \pm 0.089$

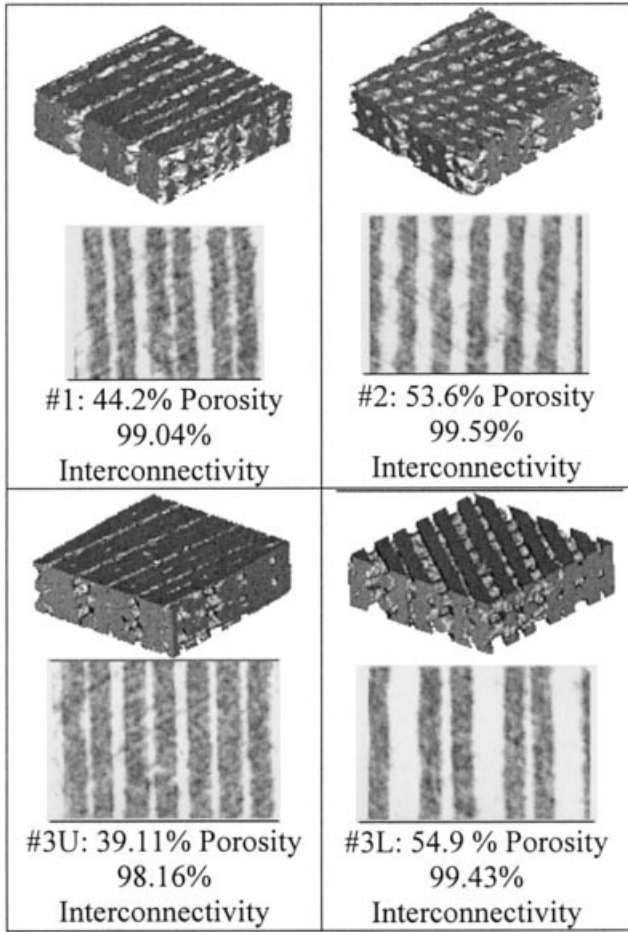


Figure 5. Reconstructed models from micro-CT imaging.

noncylindrical, compressed consistently in one axis by approximately 5% or 1 mm. Although some handling was necessary to remove the samples from the mounts on which they were constructed, this 1-mm compression is more likely a result of manufacture given the rigidity of the polymer and

the consistency of the deformation. The 2D-Relative Area, the average of relative area over 10 random samples, was found in each case to match the computed 3D volume fraction. This suggests that the relative area is consistent over many slices with few outliers. The standard deviation of less than 2.49% supports this conjecture. The porosity corresponding to each volume fraction, equal to one minus the volume fraction, is also displayed in Table II.

2D serial slices were measured for individual strut and pore widths using the 1D measurement aspect of Tview. Ten measurements were taken for each sample, and the results are displayed in Table II. Strut width is consistent between samples due to the consistency of the aperture of the nozzle used in their manufacture. Pore size is distinctly more variable, as one of the parameters differentiating the microarchitectures was the distance between individual strut deposition.

Images (200 × 200) were cropped from 62 consecutive slices in the core of each sample, and these images were reconstructed using Mimics software. The reconstructed models are displayed in Figure 5, with a sample of corresponding 2D images and the porosity and interconnectivity of each core sample. All samples showed greater than 98% interconnectivity, the majority of the pore space consisting of regular channels. The unconnected pore space consisted largely of hollows in individual strands. Upon visual inspection, there were no incidences of >100 micron pores or hollows unconnected with the rest of the channel network. As the voxel resolution of the model was 19.1 microns, this indicates that the minimum pore diameter of the interconnected region was of that same scale, sufficient for cells to migrate through. The interconnectivity models are displayed in Figure 6. The models were outlined to increase the clarity of unconnected space, consisting mostly of single pixels.

Figure 7 displays the optical images taken of the preliminary cell culture experiment. Figure 7(a) shows the confluent layer of cells atop the sample lacking the fibrin filler. The cells inside individual pores were not visible in the unfilled

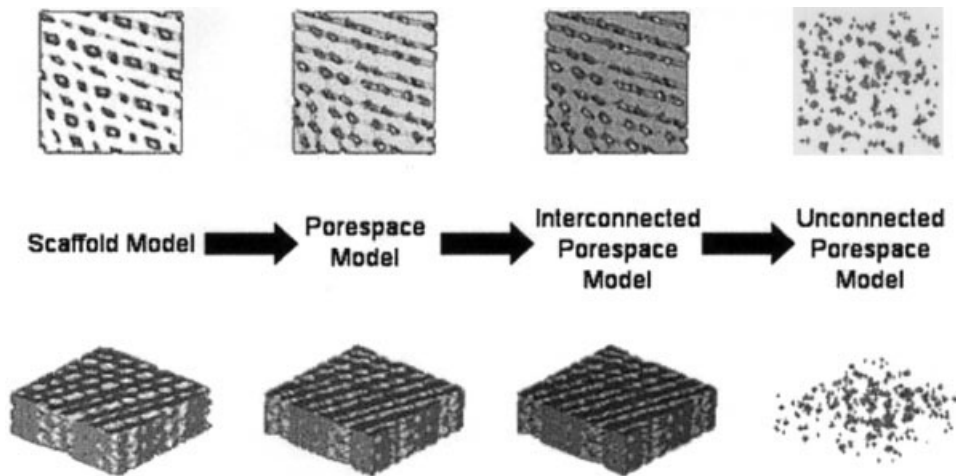
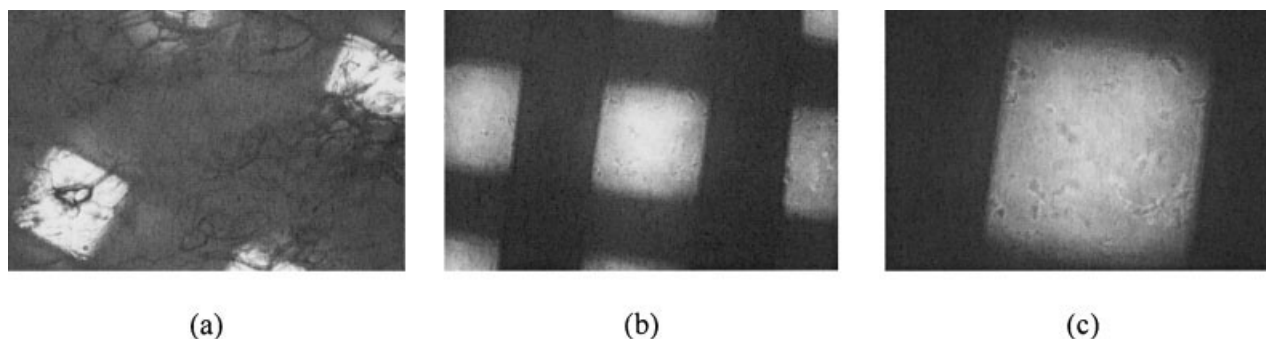


Figure 6. Pore space interconnectivity.



**Figure 7.** Images of preliminary cell culture: (a) cells growing confluent on the surface of an unfilled sample, (b) a low-resolution image of the fibrin-filled sample, and (c) a magnified view of a single pore.

sample. Figure 7(b, c) displays a single pore of the fibrin-filled scaffold at different resolutions. The cardiomyoblasts can clearly be seen inside the pore, with a greater concentration around the edge of each pore.

## DISCUSSION AND CONCLUSION

Micro-CT is capable of nondestructively imaging polymer scaffolds for the salient structural features for tissue engineering. The use of 2D analysis and 3D reconstruction software allows measurement of porosity, pore size, pore interconnectivity, and the internal layout of the scaffolds. As was illustrated with this sample, micro-CT is specifically able to measure these criteria at the scales necessary for tissue engineering work. The micro-CT scan imaged pores from 200–300 microns in these samples, near the optimal size suggested for tissue scaffolds. In a similar project using fused deposited PCL, Huang et al. reported growth of chondrocytes in a scaffold with  $65 \pm 4\%$  porosity with a pore size of 380 microns.<sup>13</sup> By comparison, sample 2 had a porosity of 52.6%, with an average pore size of 254 microns. The strut size was consistent among all samples, between 250 and 270 microns, with small standard deviations within each sample. The implication is that with regular strut size; porosity may be readily controlled simply by spacing the struts at different intervals.

The greatest asset of these samples was the porous interconnectivity of greater than 98%. The unconnected pore-space, when inspected qualitatively, appeared to consist of only small cavities within individual struts, the largest being only 30 microns across. Such interconnectivity would be extremely valuable for perfusion and cell migration throughout a scaffold. The mechanism of determining interconnectivity through 3D reconstruction of porespace and subsequent region growing performed robustly in the analysis of these four samples.

Porosity has a direct relationship to surface area, but the correlation can be difficult to compute in a complex sample. As per Table II, actual surface area of the scaffold may be determined through Tview 3D analysis. Coupled with an attachment study of PCL, this may prove valuable in deter-

mining the maximum cell density in such a scaffold. The confluent cell population per unit area may be determined from culture on bare PCL surfaces. Subsequently, extrapolation to the surface area of the 3D sample confers knowledge of the maximum cell number that may attach to PCL surfaces. Cell proliferation beyond this number indicates that cells are growing into the porespace.

In addition, the resolution of the micro-CT images was significantly finer than minimal pore size, enabling 3D reconstruction and determination of the pore interconnectivity. Therefore, for radiopaque polymers, micro-CT may prove an optimal modality for biological scaffold characterization or inspection. Radiopacity may not be a limit in and of itself, as iodinated or heavy metal contrast agents are capable of inducing radiopacity. This effect may be further exploited through the use of metal-bearing immunoassays. By utilizing the X-ray absorption features of metal particles attached to immunoglobins, micro-CT may find utilization in characterizing not only scaffold material, but also postculture tissue samples.

The simple cell culture test revealed that the PCL was still biocompatible after possible chemical changes caused in heating. In addition, the use of fibrin as a filler material was shown to allow cells to cross the pore gaps, rather than simply clinging to the pore walls. This may prove a powerful technique, using PCL as a rigid structural material while placing a bioactive but weaker material in the pore spaces. Even without filler, though, the porous PCL alone proved to be a biocompatible environment for cell culture.

The authors acknowledge Dr. Selcuk Guceri and Dr. Feng Wang at Drexel University for assistance in assembling samples.

## REFERENCES

1. Freyman TM, Yannas IV, Gibson LJ. Cellular materials as porous scaffolds for tissue engineering. *Prog Mater Sci* 2001; 46:273–282.
2. Murphy, W, Dennis RG, Kileny JL, Mooney DJ. Salt fusion: An approach to improve pore interconnectivity within tissue engineering scaffolds. *Tissue Eng* 2002;8:43–52.
3. Ma PX, Choi J. Biodegradable polymer scaffolds with well-defined interconnected spherical pore network. *Tissue Eng* 2001;7:23–33.

4. Yang S, Leong K, Du Z, Chua C. The design of scaffolds for use in tissue engineering. Part 1. traditional factors. *Tissue Eng* 2001;7:679–689.
5. Bellini A. Fused deposition of ceramics: A comprehensive experimental, analytical and computational study of material behavior, fabrication process and equipment design. Ph.D. dissertation, Mechanical Engineering, Drexel University; 2002.
6. Ng KW, Hutmacher DW, Schantz JT, Ng CS, Too HP, Lim TC, Phan TT, Teoh SH. Evaluation of ultra-thin poly( $\epsilon$ -caprolactone) films for tissue-engineered skin. *Tissue Eng* 2001;7:441–455.
7. Engelberg I, Kohn J. Physicomechanical properties of degradable polymers used in medical applications—A comparative study. *Biomaterials* 1991;12:292–304.
8. Suggs LJ, Mikos AG. Synthetic biodegradable polymers for medical applications. In: Mark JE, editor. *Physical properties of polymers handbook*. New York: American Institute of Physics; 1996. p 615–624.
9. Wang F, Shor L, Starly B, Darling A, Guceri SI, Sun W. Fabrication of poly- $\epsilon$ -caprolactone (PCL) scaffolds by precision extruding deposition process. 29<sup>th</sup> Annual Northeast Bioengineering Conference, Newark, NJ; 2003.
10. Skyscan. Skyscan 1072 desktop x-ray microtomograph: Instruction manual. Aartselaar, Belgium: Skyscan; 2001.
11. Muller R, Matter S, Neuenschwander P, Suter UV, Ruegsegger P. 3D micro-tomographic imaging and quantitative morphometry for the nondestructive evaluation of porous biomaterials. *Mater Res Soc Symp Proc* 1997;461:217–222.
12. Lin ASP, Barrows TH, Cartmell SH, Guldborg RE. Microarchitectural and mechanical characterization of oriented porous polymer scaffolds. *Biomaterials* 2003;24:481–489.
13. Huang Q, Goh JCH, Hutmacher DW, Lee EH. In vivo mesenchymal cell recruitment by a scaffold loaded with transforming growth factor b1 and the potential for in situ chondrogenesis. *Tissue Eng* 2002;8:469–482.